Chemical Engineering Journal 455 (2023) 140851

Contents lists available at ScienceDirect

Chemical Engineering Journal

journal homepage: www.elsevier.com/locate/cej

Synthesis of heterogeneous metal organic Framework-Graphene oxide nanocomposite membranes for water treatment

Hesam Jafarian [a], Mostafa Dadashi Firouzjaei [a,*], Sadegh Aghapour Aktij [b,c], Amir Aghaei [b], Mohsen Pilevar Khomami [a], Mark Elliott [a,*], Evan K. Wujcik [d], Mohtada Sadrzadeh [b], Ahmad Rahimpour [b,*]

[a] Department of Civil, Environmental and Construction Engineering, University of Alabama, Tuscaloosa, AL 35487, USA
[b] Department of Mechanical Engineering, 10-367 Donadeo Innovation Center for Engineering, Advanced Water Research Lab (AWRL), University of Alberta, Edmonton, AB T6G 1H9, Canada
[c] Department of Chemical & Materials Engineering, University of Alberta, Edmonton, AB T6G 1H9, Canada
[d] Materials Engineering And Nanosensor [MEAN] Laboratory, Department of Chemical and Biomedical Engineering and the Advanced Structures & Composites Center [ASCC], The University of Maine, Orono, ME 04469, USA

ARTICLE INFO

Keywords:
Nanocomposite
Nanofiltration membrane
Water treatment
Anti-biofouling
Antifouling

ABSTRACT

Textile wastewater is one of the most challenging streams for wastewater treatment as it is heavily contaminated with solid pollutants such as dyes. Nanofiltration (NF) membranes are a promising method to protect water resources by removing dyes and other organic contaminants from wastewater. In this study, novel NF membranes composed of a thin layer of graphene oxide (GO) and Zn-based metal–organic framework (ZIF-7) nanocomposites deposited on chitosan (CTS)-coated polyethersulfone (PES) substrate were fabricated to remove DIRECT RED 16 (DR16) dyes and humic acid from synthetic wastewater. The membrane structure was characterized using a variety of characterization methods such as SEM, XPS, FTIR, AFM, EDX, and water contact angle measurements. Introducing the GO-ZIF-7 nanocomposite layer improved the surface hydrophilicity of membranes by decreasing the contact angle from 84.9 % to 64.5 % for CTS-coated and 5GO-ZIF-7 modified membranes, respectively. This resulted in a greater dye removal rate for the modified membrane (~94 %) compared to the original CTS-coated membrane (~84 %). However, the pure water flux was reduced by 11.4 % due to the introduction of additional resistance layers. Furthermore, the addition of GO-ZIF-7 enhanced the antifouling and anti-biofouling characteristics of modified membranes against various organic and biological foulants, such as sodium alginate and *Escherichia coli* (*E.coli*). Overall, the fabricated membrane showed great dye filtration, antifouling, and anti-biofouling performances, by introducing high hydrophilicity, biocidal activities, and a negative surface charge to the membrane surface.

1. Introduction

Industrial contamination of water resources is an ongoing global challenge [1], requiring diverse solutions appropriate for a given set of contaminants, removal targets, technical capabilities, wealth levels, and regulatory regimes [2,3]. The textile industry's dyeing procedures are characterized by substantial water usage and effluents with high concentrations of different colors and salts [4]. This wastewater could be recycled or utilized again through separation and concentration processes, lowering the environmental risk and mitigating water scarcity [5,6]. Conventional wastewater treatment techniques such as biological degradation, advanced oxidation, adsorption, and coagulation-flocculation are common in the textile industry [7]. However, the above methods have numerous drawbacks, including technical complexity, the potential toxicity of textile wastewaters to the microorganisms utilized in biological reactors, large quantities of chemicals required for effective treatment, and toxic disinfection byproducts [8].

In comparison to conventional techniques, the treatment of textile wastewater by membrane-based technologies may be more straightforward and environmentally benign [9,10]. Loose nanofiltration (NF) membranes have numerous potential advantages for removing dyes from wastewater, including superior selectivity, energy efficiency,

* Corresponding authors.
E-mail addresses: mdfirouzjaei@crimson.ua.edu (M. Dadashi Firouzjaei), melliott@eng.ua.edu (M. Elliott), arahimpo@ualberta.ca (A. Rahimpour).

https://doi.org/10.1016/j.cej.2022.140851
Received 25 August 2022; Received in revised form 2 December 2022; Accepted 5 December 2022
Available online 6 December 2022

charged surfaces, and cost-effectiveness [11]. However, the main challenges with NF operations are membrane fouling and biofouling, which impair membrane performance [12]. Biofouling is thought to be more complex than chemical and inorganic fouling because extracellular polymeric substances (EPS) can form robust biofilms when microbes bind to membrane surfaces [13]. The accumulation of biofilms on the membrane surface can prevent oxidizing agents from inactivating the microorganisms and removing the biofilms [14]. Functionalization of membrane surfaces with antimicrobial nanomaterials such as MXenes [15], silver or copper nanoparticles [16], graphene oxide (GO) [17], and metal–organic frameworks (MOFs) [18–20] has been shown to prevent or slow biofilm formation [21].

Graphene oxide (GO) nanosheets are monolayers of carbon atoms organized in a tight honeycomb lattice with functional groups that are abundant in carboxyl, hydroxyl, and epoxy [22]. GO is a promising filler in functionalized nanocomposite membranes due to its high hydrophilicity, specific surface area, and reactive sites for chemical reactions [22]. However, they have a high propensity to aggregate, which can impair the performance of the membrane [23]. One promising alternative for synthesizing GO based-functional membranes is heterogenous nanocomposites of GO, such as GO-metal–organic frameworks (MOFs)-based nanocomposites [24–27].

MOFs are porous materials with crystalline structures composed of numerous organic ligands and metal clusters [28,29]. MOFs have shown exceptional biocidal properties due to controlled ion release [30,31]. Therefore, MOFs could be a viable option for modifying GO nanosheets to improve their antimicrobial properties. Researchers have examined a few GO-MOF nanocomposites to enhance the membrane's features,

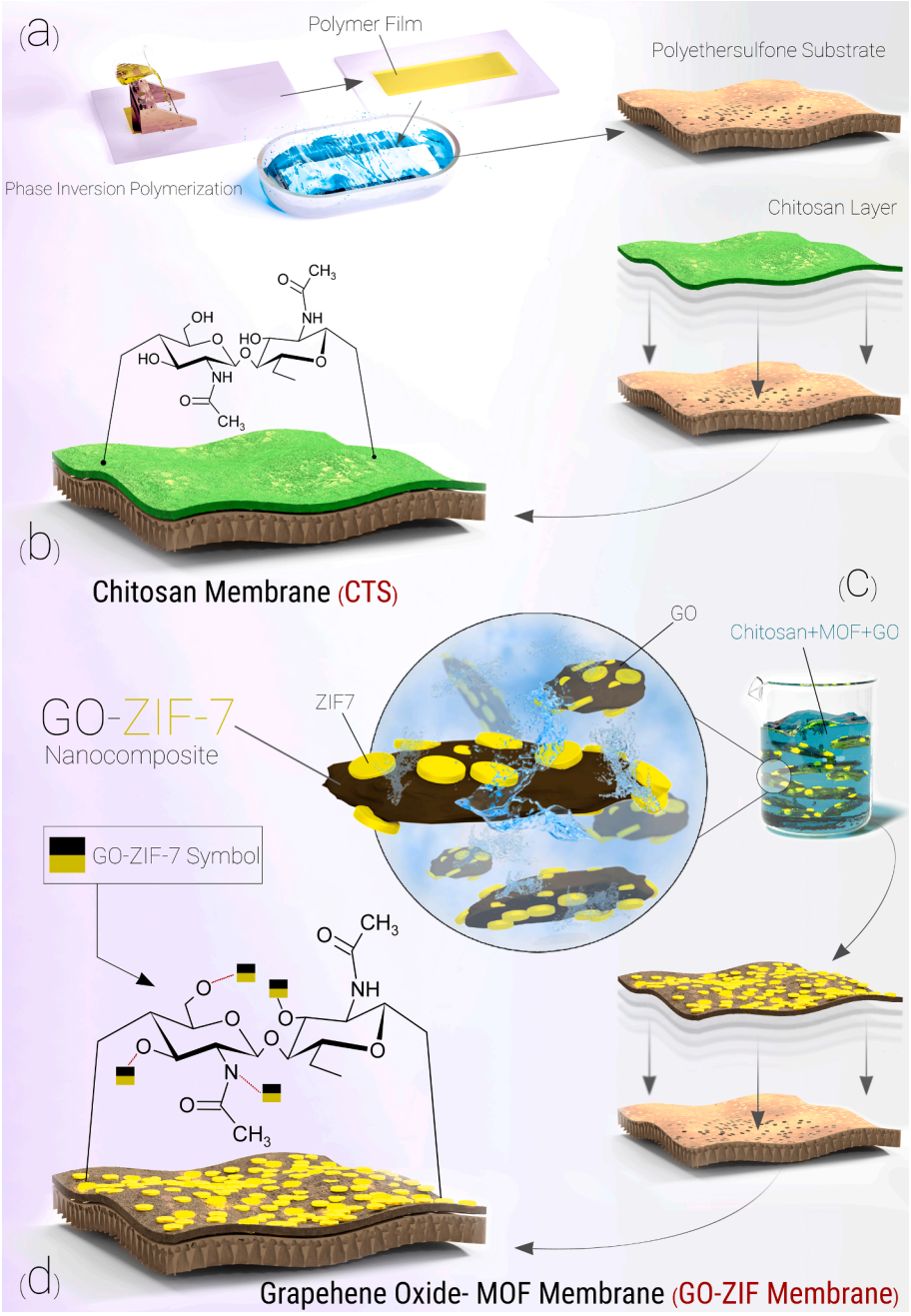

Fig. 1. The schematic illustration of PES and GO-ZIF-7 membrane fabrication process. (a) PES substrate fabrication. (b) the chemistry and structure of the CTS membrane. (c) chitosan, MOF, and GO nanocomposite polymer solution for the fabrication of GO-ZIF-7 membranes. (d) the chemistry and structure of GO-ZIF-7 membrane.

particularly its antifouling and anti-biofouling capabilities [17,32]. Yang et al. [33] created a fouling-resistant nanocomposite membrane to remove dye from wastewater using GO nanosheets and samarium-MOF that rejected more than 91 % of Rhodamine B and methylene blue dyes. Moreover, Zhang et al. [34] have utilized an ultrathin-reduced GO/MOF composite membrane to effectively remove negatively charged Congo red and positively charged methylene blue dyes. For this purpose, they have intercalated the UiO-66-$(COOH)_2$ into partially reduced GO sheets to prepare an ultrathin UiO-66-$(COOH)_2$/prGO membrane for low-pressure nanofiltration tests. The synthesized membrane illustrated high rejection yields for both Congo red (98.2 ± 1.7 %) and methylene blue (92.55 ± 2.5 %) while maintaining a permeability of 20 ($L.m^{-2}.h^{-1}.bar^{-1}$). Most recently, Alemayehu et al. [35] have investigated the Congo red rejection by a novel composite membrane synthesized via the integration of Al-MOF nanosheets into the GO structure. The fabricated composite membrane (GO@Al-MOF) obtained excellent rejection (99.9 %) and permeability (51.6 $L.m^{-2}.h^{-1}.bar^{-1}$) under nanofiltration. However, it should be noted that the fouling and biofouling behavior of the membrane was not investigated. Thus, the long-term stability of the GO@Al-MOF membrane is yet to be evaluated.

In this study, zeolite imidazolate framework (ZIF-7) was chosen as the MOF component of the nanocomposite membrane, because of the great biocidal activities of zinc. Therefore, a hydrophilic GO-ZIF-7 nanocomposite with a high surface charge was incorporated into the chitosan-coated polyethersulfone (PES) membrane for the first time. The main objective of this study was to optimize the concentrations of the nanocomposite components to achieve high rejection of DIRECT RED 16 (DR16) dyes and humic acid from synthetic wastewater. The pure water flux and dye rejection of membranes were investigated using an NF setup. Moreover, all blank and modified membranes were evaluated for their antifouling and anti-biofouling capabilities against organic and biological foulants.

2. Materials and methods

2.1. Reagents and materials

Polyethersulfone (PES, M_w = 58000 g/mol, Ultrason E6020P), N, N dimethylformamide (DMF, Scharlau), Triton X-100 (Merck), and polyvinyl pyrrolidone (PVP, M_w = 25000 g/mol, Merck) were utilized to prepare the support membrane. Chitosan powder (CTS, medium molecular weight, Orbital), glacial acetic acid (Merck), sodium hydroxide (NaOH, Merck), polyethylene glycol (PEG 6000, Scharlau), sodium tripolyphosphate (TPP, Across), graphene oxide (GO, 50 mg/ml, dispersion in H_2O), zinc nitrate hexahydrate ($Zn(NO_3)_2$.62GO-ZIFO, M_w = 297.49 g/mol, Sigma-Aldrich), and benzimidazole ($C_7H_6N_2$, Merck) were used for the synthesis of the modified membranes (GO-ZIF-7 incorporated in a CTS-coated PES membrane). The azo dye, Direct Red 16 (DR16, $C_{26}H_{17}N_5Na_2O_8S_2$, 99 wt%, M_w = 637.26), purchased from Sigma Aldrich, USA, was used to assess the dye rejection performance of the membranes. Humic acid (HA, Across), *Escherichia coli* (*E. coli*, ATCC 25922), sodium alginate (SA, Sigma-Aldrich), potassium phosphate (KH_2PO_4, Merck), sodium chloride (NaCl, Merck), magnesium sulfate ($MgSO_4$, Merck), sodium bicarbonate ($NaHCO_3$, Merck), calcium chloride ($CaCl_2$, Merck), and ammonium chloride (NH_4Cl, Merck) were used to prepare synthetic wastewaters used in fouling and biofouling measurements.

2.2. Synthesis of GO and GO − ZIF-7 nanocomposites

In a flask of concentrated sulfuric acid (95 %, 50 ml), graphite powder (1 g) was added, followed by a total of 3 g of potassium permanganate, which was added three times to prevent the temperature from rising rapidly. After heating the flask to 40 °C for 6 h, crumbling ice containing H_2O_2 (30 wt%, 10 ml) was poured over the GO slurry. After one week of diffusion dialysis, the dark green slurry was turned to the dark brown slurry, and the resultant suspension was filtered over a polytetrafluoroethylene membrane. The remaining solid was thoroughly washed with 1 M HCl, followed by acetone and water. The GO powder was obtained by freeze-drying at −60 °C for 24 h. Finally, the GO dispersion in deionized water was obtained at the concentration of ~ 50 mg/ml and used for device applications.

To synthesize GO − ZIF-7 nanocomposites, GO (0.1 g) was initially dispersed in 40 ml of deionized (DI) water using sonication for 20 min at room temperature, followed by 24 h of vigorous stirring. Then, zinc nitrate hexahydrate (0.446 g) was dissolved in 30 ml of DI water and added to the GO solution. The obtained mixture was continuously stirred for 6 h. Next, 0.354 g benzimidazole was dissolved in 30 ml of ethanol and mixed with the previous solution. The final mixture was stirred for 2 h, followed by 2 h of settlement. After that, the rich solution was decanted and rinsed with 100 ml of ethanol to remove the unreacted substances. The formed nanocomposites were centrifuged for 15 min at 8500 rpm. Finally, GO-ZIF-7 nanocrystals were placed in an oven at 60 °C for 6 h to eliminate the residual solvents.

Table 1
The summary of membranes' labeling and structure information.

Membrane Name	PES Substrate	Chitosan Layer	GO-ZIF-7 Concentration (%)
PES	✓	✘	0
CTS	✓	✓	0
2GO-ZIF	✓	✓	2
5GO-ZIF	✓	✓	5
8GO-ZIF	✓	✓	8

2.3. Preparation of nanocomposite membranes

The porous PES blank support membrane was fabricated through a non-solvent-induced phase inversion technique. The PES solution (14 wt % PES, 2 wt% Triton X-100, 1 % wt. PVP, and 86 wt% DMF) was cast on a clean glass plate with a casting knife (100 μm gate height) followed by immersion in a water coagulation bath at room temperature. Layers of CTS and CTS/GO-ZIF-7 were then dip-coated on the PES substrate. CTS powder (0.5 g) was dissolved in 75 ml of aqueous acetic acid 2 % (v/v) for 1.5 h at 80 °C. Then, a solution comprised of PEG 6000 (0.1 g) and DI water (25 ml) was added to the CTS solution. Moreover, CTS/GO-ZIF-7 solutions were prepared by gradually adding various GO concentrations (2, 5, and 8 wt%) to the CTS solution. The final solution was sonicated for 20 min at room temperature. Afterward, it was continuously stirred for 1 h to achieve homogeneous dispersion.

The schematic of modifying the membrane surface with nanocomposite coating is provided in Fig. 1. The modified membranes were prepared by soaking PES substrates into CTS and CTS/GO-ZIF-7 solutions for 2 min. The immersed substrates were then placed in the oven at 80 °C for 15 min to remove the residual solutions from the surface. Next, the cross-linking reaction proceeded by dipping the membranes into a solution containing TPP (0.5 g) and DI water (200 ml) for 5 min. After that, the membranes were immersed in an aqueous NaOH 2 % (v/v) solution for 30 min. Finally, the modified membranes were washed with DI water to remove residuals and dried to the ambient temperature. The fabricated membranes were labeled as blank (primitive PES membrane), CTS (chitosan@PES), 2GO-ZIF (2 %GO-ZIF-7@CTS@PES), 5GO-ZIF (5 %GO-ZIF-7@CTS@PES), and 8GO-ZIF (8 %GO-ZIF-7@CTS@PES). Table 1 describes the membrane label and ingredients.

2.4. Characterization of the nanocomposites and membranes

X-ray photoelectron spectroscopy (XPS, Axis 165 XPS/ Auger, Shimadzu, Japan) and attenuated total reflection-Fourier transform infrared spectroscopy (ATR-FTIR, ThermoNicolet NEXUS 870, USA) were employed to analyze the chemical structures of the synthesized

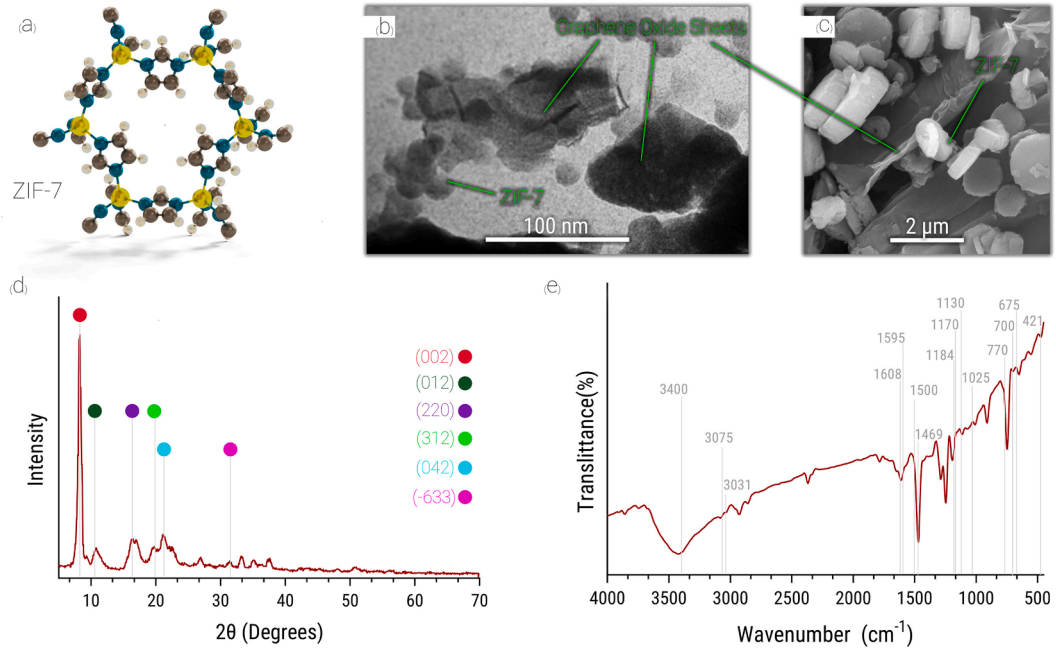

Fig. 2. (a) Schematic chemical structures of ZIF-7. (b) the TEM images of GO-ZIF-7. (c) SEM image of GO-ZIF-7 nanocomposites. (d) XRD pattern and (e) FTIR spectra of GO-ZIF-7 nanocomposites. The simulated XRD of the ZIF-7 is provided in supporting information.

nanocomposites and membranes. X-ray powder diffraction (XRD) patterns were recorded at 25 °C using an X'Pert Pro X-ray diffractometer equipped with a Cu Kα radiation in 2θ mode from 0° to 70° to define the crystalline structure of the nanoparticles. Field emission scanning electron microscopy (SEM, JEOL FE 7000, JEOL, USA) equipped with an energy-dispersive X-ray (EDX) spectrometer was used to study the morphology of the synthesized nanocomposites and membranes. The surface topology and roughness of the membranes were investigated using atomic force microscopy (AFM, Bruker Dimension Icon, USA). In this regard, the roughness parameters were measured over a sample size of 10 µm × 10 µm. A contact angle analyzer (Krüss GmbH, Germany) was employed to assess the surface wettability of the modified membranes. Five random points were measured for each sample to minimize the experimental error.

2.5. Membrane performance evaluation

2.5.1. Pure water flux process

A dead-end NF setup was used to measure the pure water flux of the membranes. The compressed N_2 gas regulated the pressure. The membranes were compacted by pure water filtration at 4 bar for 45 min before the filtration experiments. The efficient membrane area, time interval, and pressure of the system were 23.8 cm^2, 20 min, and 3 bar, respectively. The permeate flux (J_w) was calculated using the following equation [36]:

$$J_w = \frac{V}{A.\Delta t} \tag{1}$$

where V (L) is the permeate volume, A (m^2) is the effective membrane area, and Δt (h) is the filtration time.

2.5.2. Dye filtration experiments

Aqueous solutions containing 100 ppm of DR16 were used to determine the dye rejection performance of the modified membranes. The permeate samples were collected after 20 min. A magnetic stirrer was used to mitigate the concentration polarization effects during the filtration. The dye concentration of both feed and permeate was determined by UV–vis spectrophotometer at 527 nm (λ_{max}) corresponding to DR16. The following equation was applied to calculate the dye rejection (R) [36]:

$$R(\%) = (1 - \frac{C_p}{C_f}) \times 100 \tag{2}$$

where C_p and C_f are the permeate and feed concentrations, respectively.

2.6. Assessment of antifouling and anti-Biofouling properties

Antifouling and anti-biofouling properties of the membranes were evaluated using an NF cross-flow system at 25 °C. The pressure and feed velocity of the system were set to 3 bar and 12.5 cm/s, respectively. The antifouling performance of the membranes was investigated using three different synthesized feeds; a) DR16 in DI water (100 mg/L), b) sodium alginate (250 mg/l) dissolved in DI water (3.5 L), and c) NaCl (0.4 mM), $NaHCO_3$ (0.2 mM), $CaCl_2$ (0.3 mM), and humic acid (30 mg/l) dissolved in DI water (4L).

The system was first cleaned with ethanol 70 % (v/v), followed by washing with DI water to evaluate the anti-biofouling performance of the modified membranes. For this purpose, a synthetic wastewater solution containing NH_4Cl (0.93 mM), $NaHCO_3$ (0.5 mM), $MgSO_4$ (0.61 mM), KH_2PO_4 (0.45 mM), NaCl (9.2 mM), and $CaCl_2$ (0.5 mM) was prepared. Then, a suitable amount of *E.coli* was added to the prepared solution to achieve a primary concentration of approximately 10^7 CFU/mL.

After measuring the initial pure water flux (J_{w1}), the membranes were cleaned with DI water through the feed channel for 45 min to calculate the flux recovery ratio. Then, the pure water flux was measured again at the same condition (J_{w2}). The following equation was used to calculate the flux recovery ratio [36]:

$$FRR(\%) = \frac{Jw_2}{Jw_1} \times 100 \tag{3}$$

2.7. Sustainability test of the membranes

Membrane coupons (4 cm^2) were stored overnight in DI water (20 ml) under mild shaking to measure the release rate of the zinc ion in the nanocomposite layer of the modified membrane. Then, the coupons

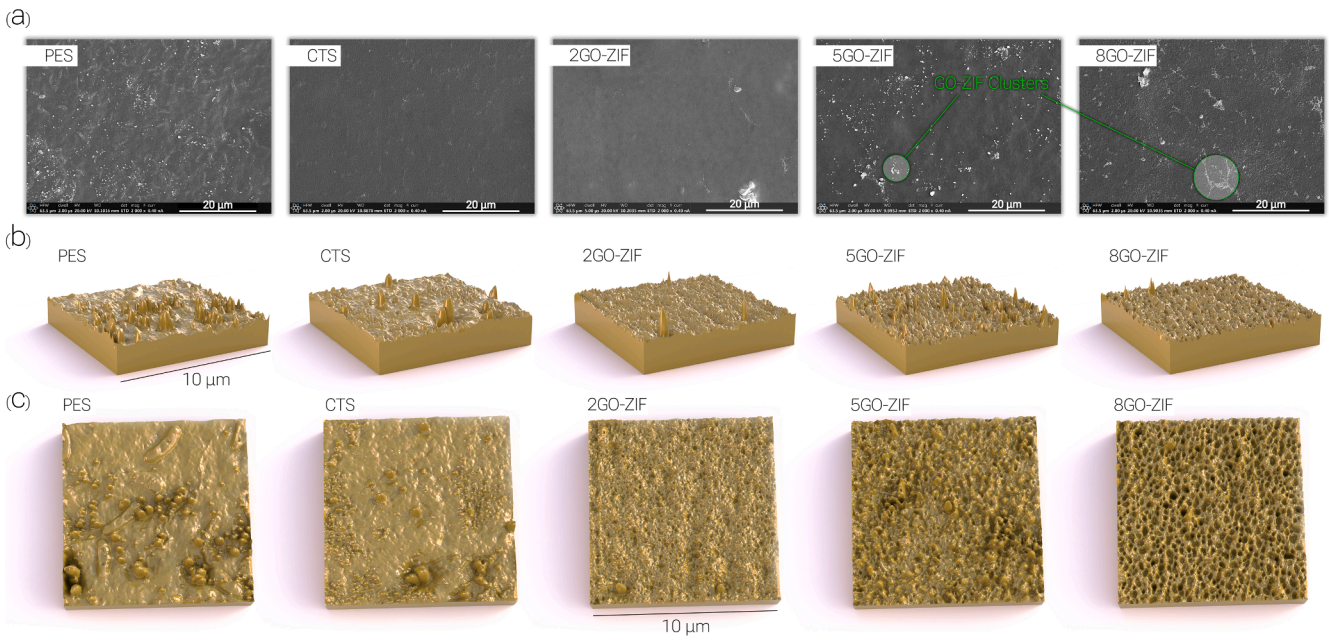

Fig. 3. (a) The top surface SEM images of the blank and GO-ZIF membranes. (b) The cross angle, and (c) top angle 3-dimensional AFM images of membranes.

were acidified using nitric acid 1 % (v/v) and shaken at 80 rpm for 16 days. Water samples and the modified membranes were analyzed after 1, 6, and 16 days. The concentration of the leached zinc ions was determined using an inductively coupled plasma-optical emission spectrometer (ICP-OES, Thermo iCAP6300 Duo, Thermo Fisher, USA).

3. Results and discussion

3.1. Characterization of the GO-ZIF-7 nanocomposites

The structure of ZIF-7 and GO-ZIF-7 nanocomposite is shown in Fig. 2**a and b**. ZIF-7 nanoparticles were uniformly dispersed inside the GO structure while preserving their structural shape, as seen by the TEM images (Fig. 2**b**). The distribution of narrow-size and homogeneous ZIF-7 nanoparticles in the GO structure is also shown in SEM images (Fig. 2**c**). It can be shown that the ZIF-7 crystals in the GO framework are in cubic or rectangular shapes without any significant aggregation. After being combined, the GO and ZIF-7 nanoparticles kept their structural forms consistent with the TEM findings.

The formation of ZIF-7 on the GO structure is supported by the XRD patterns of the nanocomposites (Fig. 2**d**). According to XRD patterns, the (002) crystalline plane of GO with a d-spacing of 1.07 nm showed a sharp and powerful peak at $2\theta = 8.25°$ [37]. Additionally, peaks near 2θ = 10.45, 16.45, 16.95, 19.8, 21.2, 22.51, and 31.45 are related to the (012), (220), (−132), (312), (042), (−243), and (−633) crystalline planes of ZIF-7, confirming the successful synthesis of GO-ZIF-7 [38,39]. The FTIR spectra of the created nanocomposites are displayed in Fig. 2**e**. The peaks at 3400 cm^{-1} (OH stretching mode), 1025 cm^{-1} (C—O epoxy), 1184 cm^{-1} (hydroxyl group of tertiary C-OH), and 1608 cm^{-1} (hydroxyl group of carbonyl) are assigned to GO [40]. The peaks at 1130 and 1170 cm^{-1} (CO), 675–770 cm^{-1} (CH), 700–1500 cm^{-1} (imidazole ring in both modes of stretching and bending), 1610 cm^{-1} (C═N stretch mode), and 3031 and 3075 cm^{-1} (=CH stretching mode in the aromatic ring) are assigned to ZIF-7 [41]. The peak at 421 cm^{-1} further validates the stretching of the Zn-N bond [41].

3.2. Physicochemical properties of membranes

SEM images were used to investigate the morphologies of unmodified and modified membranes (Fig. 3**a**). CTS formed a relatively uniform layer over the asymmetric structure of the PES substrate. However, after adding GO-ZIF-7 nanocomposites, the surface morphology altered and

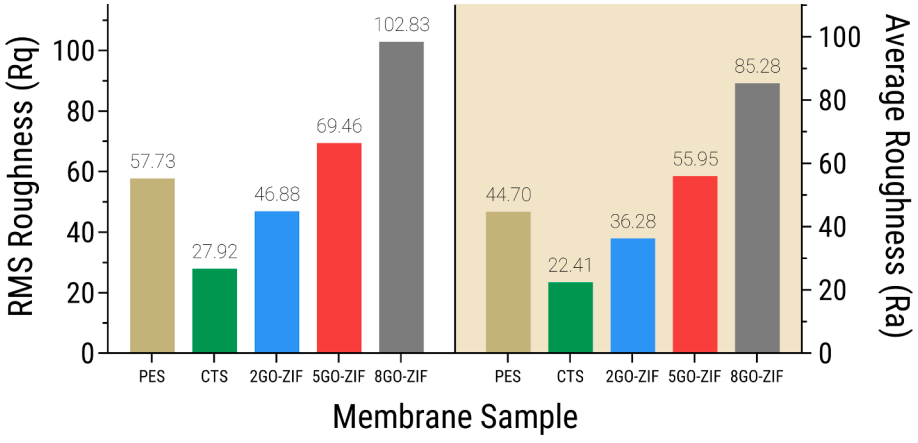

Fig. 4. The roughness values of root-mean-square (Rq) and average roughness (Ra) were calculated from AFM images using at least three different locations on each membrane sample.

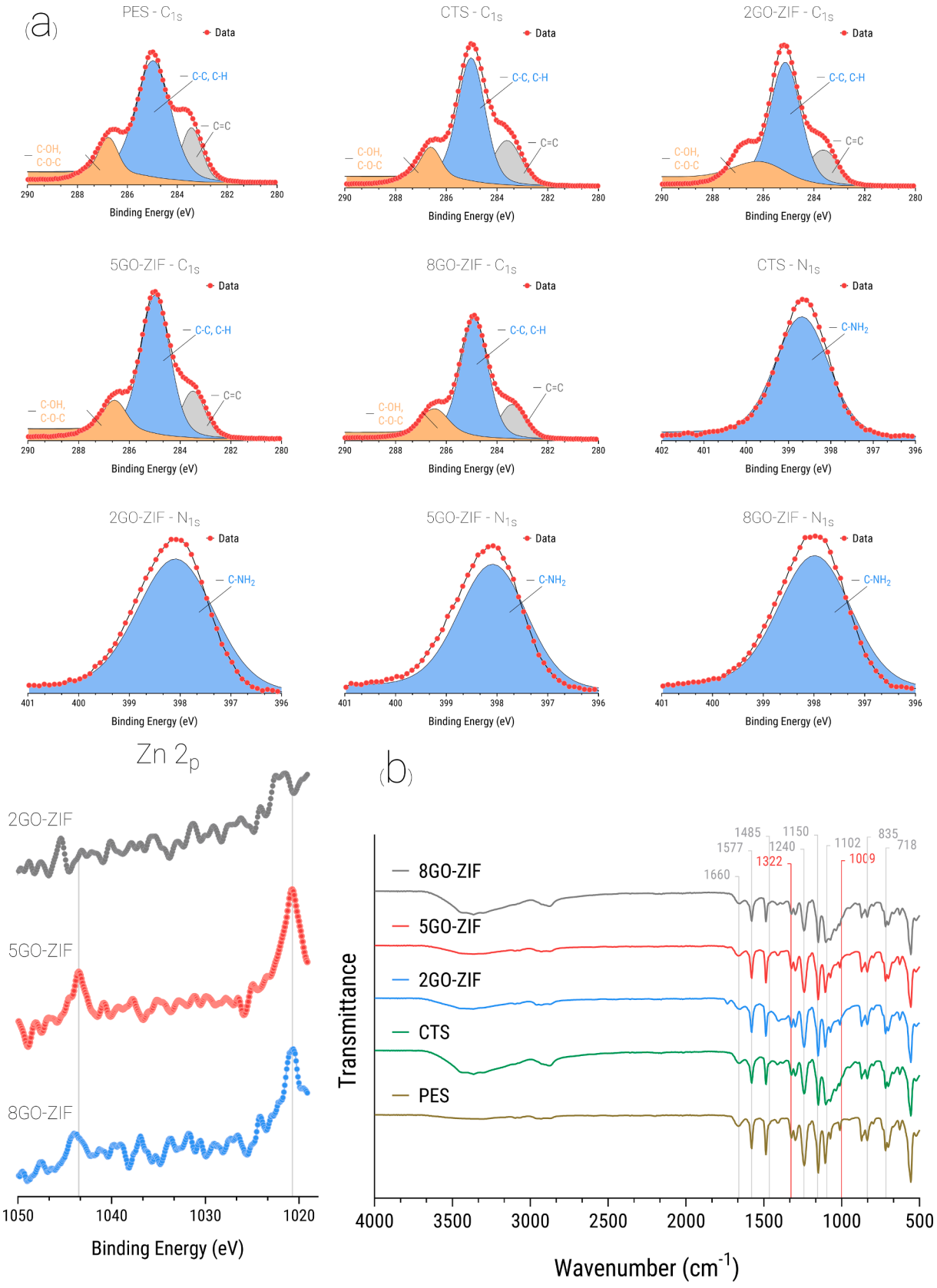

Fig. 5. XPS survey spectra of the membranes. (a) Deconvoluted high-resolution XPS spectra of C 1 s, N 1 s, Zn 2p, and (b) FTIR spectra of the membranes. The gray and red line are to help the reader to better locate the characteristic peaks.

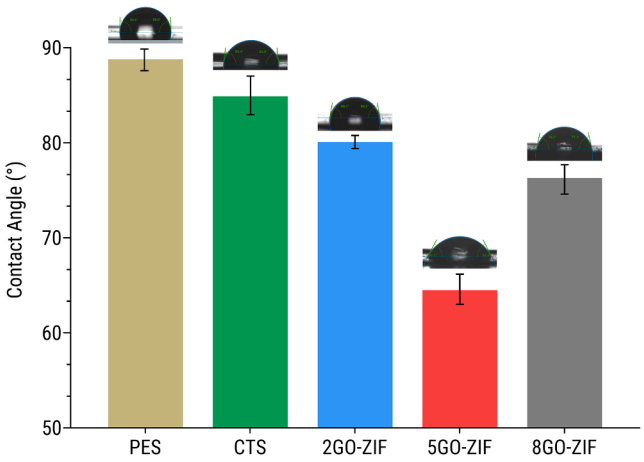

Fig. 6. Contact angle measurements of water sitting on the surface of the various membranes with real time photo of the water droplets.

some noticeable wrinkles and grooves emerged. The GO-ZIF-7 decorated membranes had a thicker active layer and rougher surface than the CTS membrane, as shown by SEM micrographs. The positively charged Zn ions of ZIF-7 nanocrystals can interact with anchor sites provided by CTS catechol functional groups.

AFM was utilized to evaluate the changes in membrane surface roughness after modification by GO-ZIF-7 nanocomposites (Fig. 3**b** and **c**). The average roughness (R_a) and root-mean-square roughness (R_q) of the unmodified and modified membranes, as well as 3D AFM images, are displayed in Fig. 3**b–d** and Fig. 4. Chitosan coating smoothed out the original PES membrane surface, showing a 51 % drop in Rq and a 49 % drop in Ra. However, adding GO-ZIF-7 to the membrane surface increased the GO-ZIF membrane's surface roughness. According to quantitative results, the R_q values of the 5GO-ZIF and 8GO-ZIF membranes have increased by more than 20 % and 44 %, respectively (Fig. 4). The results are consistent with SEM images showing a rougher surface of GO-ZIF membranes than the CTS membrane. Although higher GO-ZIF membrane roughness may negatively impact fouling and biofouling resistance, other essential factors like electrostatic charges, biocidal activities, and surface affinity to water can enhance the antifouling properties of the membrane [14].

XPS measurements were carried out to examine the elemental analysis and chemical bonding of blank and modified membranes. XPS spectra of all membranes revealed peaks at 529, 396, and 282 (Fig. 5**a**), which were associated with the predominant elements, including oxygen (O), nitrogen (N), and carbon (C), respectively [42]. The GO-ZIF membrane spectra also showed two strong zinc peaks around 1020.8 and 1043.6 eV, which are attributed to Zn $2P_{3/2}$ and Zn $2P_{1/2}$, respectively [43]. These zinc peaks show that ZIF-7 nanocrystals are present on the surface of GO-ZIF membranes. FTIR spectra were measured and shown in Fig. 5**b** to describe the chemical composition of the membranes. The PES support corresponds to the peaks at 1150 and 1322 cm^{-1} (O=S=O stretching mode) and 1240 cm^{-1} (asymmetric C—O—C stretching mode) [44]. The O—H bonds of the CTS layer may also be seen between 2926 and 3363 cm^{-1} [45]. The FTIR spectra also contain two distinctive absorbance bonds at 1660 cm^{-1} (N—H bending mode of Amide I) and 1577 cm^{-1} (C—N stretching mode of amide II) [45]. Furthermore, the cross-linking of the compounds with TPP results in vibration of the P=O stretching mode, which is indicated by the measured peak at 1150 cm^{-1} [44]. The residue peaks are found at 1485 cm^{-1} (C=C stretch mode of GO), 1102 cm^{-1} (C—H in-plane bending mode), 835 cm^{-1} (C—H out-of-plane), and 718 cm^{-1} (C—C ring out-of-plane bending) [46]. A new peak at 1009 cm^{-1} in GO-ZIF membranes can be attributed to the C—N stretching vibration [47]. According to a related study, this peak supports the successful development of GO-ZIF nanocomposite on the surface of the CTS-coated membrane.

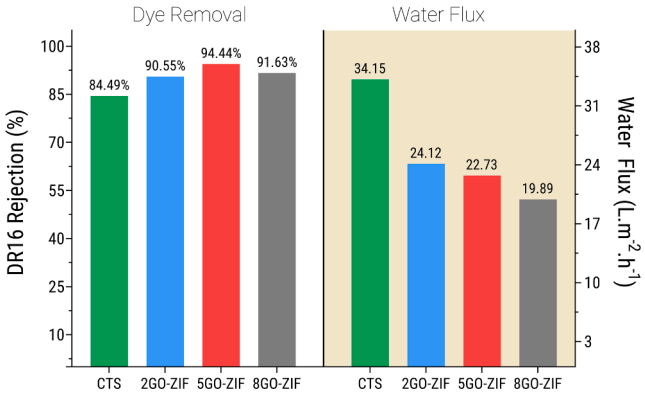

Fig. 7. Dye rejection and pure water flux of the fabricated membranes. Experiments were repeated three times and mean value is reported. The coefficient of variation was set to be below 7% for all data points.

The surface hydrophilicity significantly impacts the transport and fouling behaviors of membranes. In this regard, the contact angle measurements were made to determine the wettability of the fabricated membranes. The contact angle of the CTS membrane was slightly lower than that of the PES membrane due to the existence of a CTS layer on the surface, as seen in Fig. 6. The hydrophilic properties of the carbonyl and hydroxyl functional groups in the CTS structure may be responsible for the modest improvement in surface wettability. In comparison to PES and CTS membranes, GO-ZIF membranes showed a lower contact angle, indicating higher surface wettability and better affinity to water molecules. The key factor contributing to the GO-ZIF membranes' improved wettability may be oxygen-containing functional groups, including epoxide, hydroxyl, and carboxyl [48]. Another possible reason is the increase in surface physical heterogeneity or roughness, which enhanced surface wettability based on the Wenzel equation [49,50]. Despite GO-ZIF membranes having rougher surfaces than chitosan membranes, improved wettability may significantly reduce biofouling, dominating the impact of increased surface roughness [51]. Among the examined membranes, the membrane containing 5GO-ZIF displayed the best hydrophilicity behavior, demonstrating that the GO-ZIF-7 concentration must be optimized before coating. Overall, the likelihood of foulants sticking to the membrane surface is decreased by enhancing surface hydrophilicity, which lowers membrane fouling.

3.3. *Transport properties of the membranes*

The transport characteristics of the membranes were assessed based on the pure water flux (J_w) and dye removal results. The J_w of the CTS membrane, as shown in Fig. 7, was higher than the J_w attained for the GO-ZIF membranes. The mass transfer resistance of GO-ZIF membranes increased with thicker GO-ZIF-7 coating layers, which decreased the membrane permeance. Although adding GO-ZIF-7 nanocomposites improved the surface hydrophilicity, mass transfer resistance was the main contributor to a decrease in water permeance in GO-ZIF membranes [52]. The results also demonstrated that the deposition of GO-ZIF-7 on the membrane surface needs to be optimized as the pure water flux may be lowered with the excessive addition of GO-ZIF-7.

The GO-ZIF-modified membranes outperformed the CTS membrane in terms of dye rejection, as seen in Fig. 7. This result indicates that the incorporation of GO-ZIF-7 nanocomposites led to the formation of a selective dense layer on the membrane surface, verified by SEM data (Fig. 3). The electrostatic interactions between DR16 and the membrane surface may also be responsible for improved dye removal for the modified membranes.

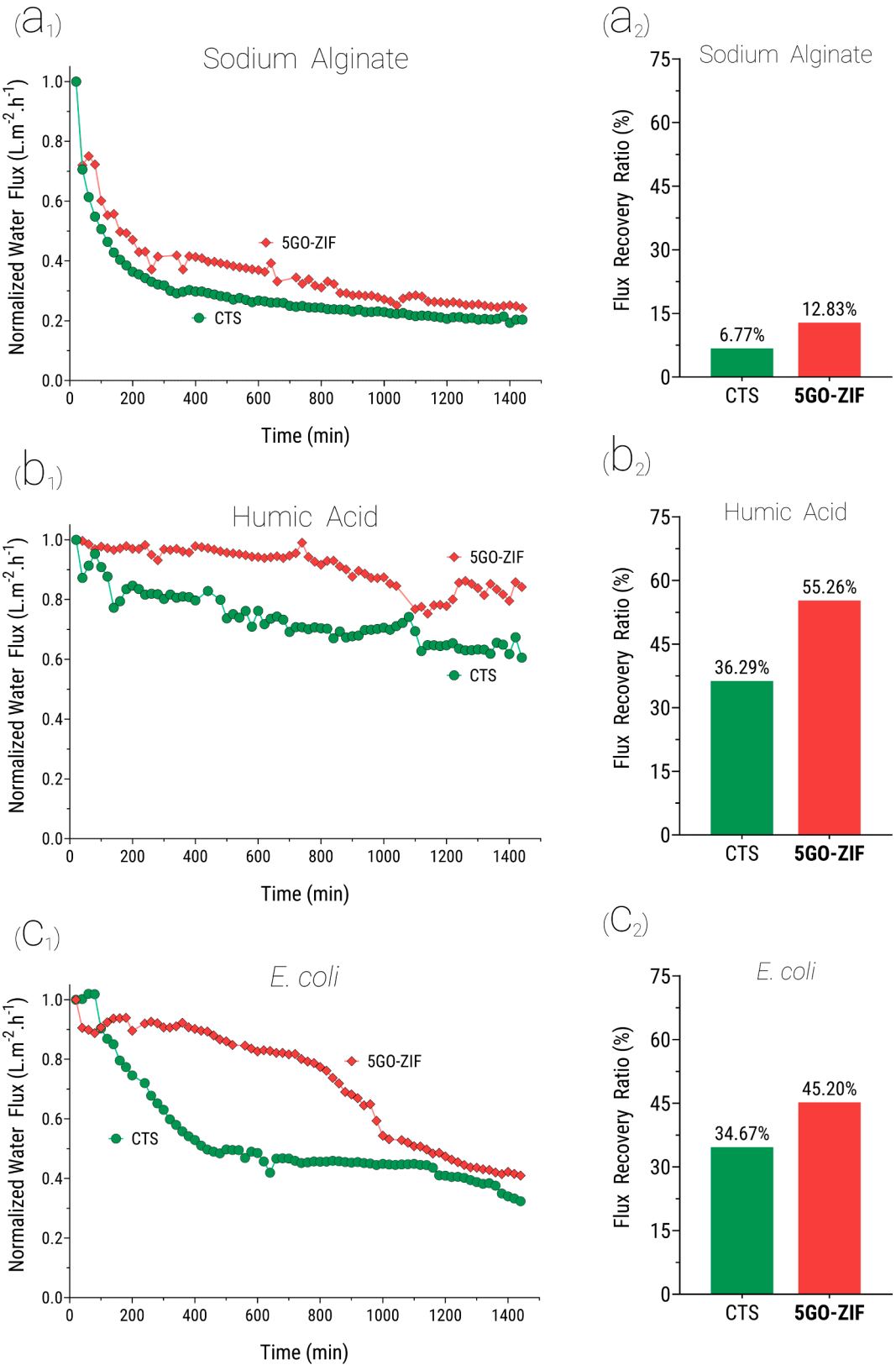

Fig. 8. Normalized water fluxes of the CTS and 5GO-ZIF membranes versus time and their flux recovery ratios for (a) sodium alginate, (b) humic acid, and (c) *E. coli*. Experiments were repeated three times and mean value is reported. The coefficient of variation was set to be below 7% for all data points.

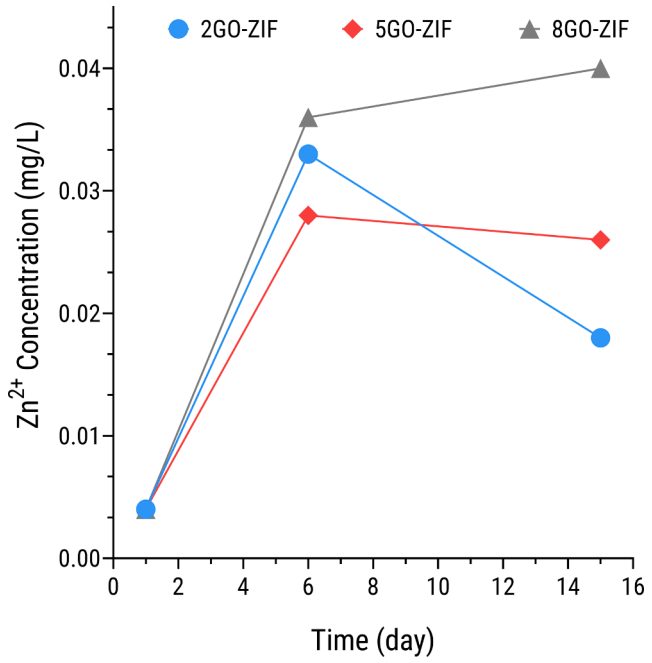

Fig. 9. Zn^{2+} leaching evaluation of the GO-ZIF membranes.

3.4. Assessment of antifouling and anti-biofouling properties of the membranes

The fouling and biofouling potential of the TFN membrane and their corresponding flux recovery ratios were assessed through the dynamic NF experiments with various feed solutions containing sodium alginate, humic acid, Direct Red 16 (DR16), and *E.coli* (Fig. 8). Fig. 8**a$_1$** illustrates the water flux through GO-ZIF modified and CTS membranes for the sodium alginate solution over time. During the long-term filtration process, most of the alginate foulant may deposit on the membrane surface, generating a fouling layer and thus leading to a more significant flux decrease. However, to further assess the antifouling effectiveness of the membranes, the flux recovery ratio was evaluated after forward-washing of the membranes for 45 min. As can be seen in Fig. 8**a$_2$**, the flux recovery of the membrane was improved (around 47 %) by introducing GO-ZIF-7 deposition.

The organic fouling performance of membranes was further assessed by feed solutions containing humic acid. As shown in Fig. 8**b$_1$**, the CTS membrane showed a flux decline of around 39 %, whereas the 5GO-ZIF membrane showed a partial reduction in the water flux of about 16 %. Additionally, the flux recovery ratio of the 5GO-ZIF membrane was improved considerably compared to the unmodified membrane (Fig. 8**b$_2$**). Similarly, the anti-biofouling property of the membrane was improved by decorating the surface with 5GO-ZIF (Fig. 8**c**). The improved surface hydrophilicity of the GO-ZIF membrane forms a hydrated layer with a reduced propensity to fouling agents. Overall, the higher surface wettability and development of a hydrated layer, which reduces the adhesion of organic foulant to the membrane's surface, are responsible for the better fouling resistance of the GO-ZIF membrane.

3.5. Sustainability test of the membranes

ICP-MS was used to measure the rate of Zn^{2+} release for the GO-ZIF membranes over 16 days. All fabricated GO-ZIF membranes showed a sharp release rate in the first six days (Fig. 9) due to the detachment of loose nanoparticles from the membrane surface. However, the GO-ZIF membranes displayed various Zn^{2+} release behaviors over time. The zinc ions can be adsorbed on the negatively charged oxygen-containing functional groups of GO, preventing the Zn-MOFs from rapid Zn^{2+} leakage. After six days, the GO-ZIF membranes released Zn^{2+} in the following order: 2GO-ZIF < 5GO-ZIF < 8GO-ZIF, suggesting that the membranes with higher content of ZIF-7 tend to release more Zn^{2+}. Furthermore, the continuous biocide-releasing to the boundary layer near the membrane surface serves as a source of biocides and forms an inhibition zone [53]. They can serve as the reservoir of biocidal metal ions and the continuous gradual release of the metal ions by biodegradation of the framework can provide sustainable antibacterial activity with high productivity, which is proved through long-term biofouling tests [54]. The cumulative Zn^{2+} content (16 days) in the examined GO-ZIF membranes was much lower than the recommended level of 3 mg/L established by the World Health Organization (WHO). The results imply that adding GO-ZIF-7 to the thin-film layer can create a stable and long-lasting Zn^{2+} reservoir to reduce membrane biofouling during prolonged filtration.

4. Conclusion

In this study, a novel nanocomposite membrane was developed to treat DR16 dyes and humic acid in synthetic wastewater. For this purpose, a PES membrane was coated by a thin film of CTS/GO-ZIF-7 using the phase inversion technique. Characteristic evaluations confirmed that incorporating GO-ZIF-7 nanocomposites in the surface elevated the roughness and hydrophilicity of the membrane. Based on the results, the dye rejection of GO-ZIF membranes was substantially higher than the CTS membrane due to the particular features of GO-ZIF-7. In this regard, the highest dye removal was achieved by the 5GO-ZIF membrane (~94 %). Moreover, the GO-ZIF layer enhanced the antifouling and anti-biofouling properties of the membrane due to the high surface hydrophilicity, and biocidal activities of GO and zinc introduced by GO-ZIF-7 nanocomposites. It should be noted that coating the 5GO-ZIF nanocomposite layer on the CTS membrane reduced the pure water flux (by

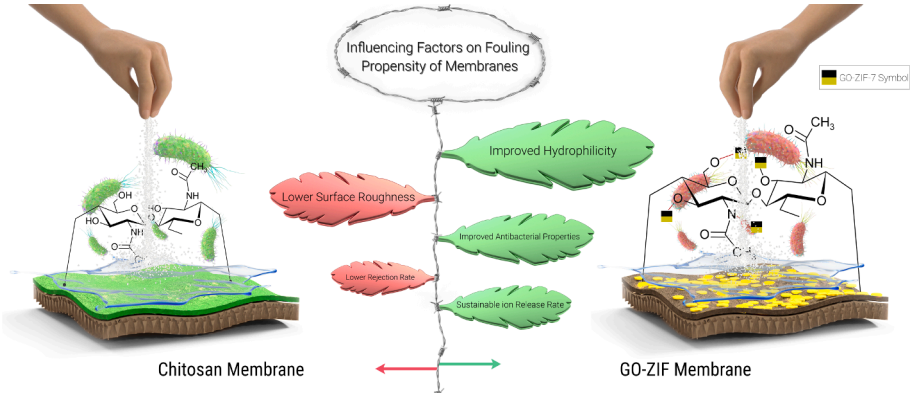

Fig. 10. Graphical conclusion of the influencing factors on the fouling propensity of the membranes.

11.4 %), which can be a limitation for practical applications in industries. The reduction in pure water flux can be explained by the increased mass transfer resistance with the addition of layers containing GO-ZIF- nanocomposite. Regarding future research topics, incorporating other types of metals into the GO-MOF structure could potentially improve the anti-biofouling performance of the membrane. It can also be effective in improving the pure water flux of the nanocomposite membrane by altering the morphology of the nanocomposite membranes. Fig. 10 provides a graphical conclusion for the affecting factors on the fouling propensity of the membranes.

Declaration of Competing Interest

The authors declare that they have no known competing financial interests or personal relationships that could have appeared to influence the work reported in this paper.

Data availability

Data will be made available on request.

Acknowledgment

This research benefitted greatly from funding provided by USDA TAT-RWTS 00-69526. This paper has not been formally reviewed by USDA and the views expressed in this document are solely those of the authors and do not necessarily reflect those of USDA. USDA does not endorse any products or commercial services mentioned in this publication. USDA had no role in the study design, data collection, analysis, decision to publish, or preparation of the manuscript.

Appendix A. Supplementary data

Supplementary data to this article can be found online at https://doi.org/10.1016/j.cej.2022.140851.

References

[1] D. Jassby, T.Y. Cath, H. Buisson, The role of nanotechnology in industrial water treatment, Nat. Nanotechnol. 13 (8) (2018) 670–672.
[2] A. Islam, et al., Ceramic membrane for water filtration: addressing the various concerns at once, Chem. Eng. J. 446 (2022), 137386.
[3] M. Dadashi Firouzjaei, et al., Chemistry, abundance, detection and treatment of per- and polyfluoroalkyl substances in water: a review, Environ. Chem. Lett. 20 (1) (2022) 661–679.
[4] R. Kishor, et al., Ecotoxicological and health concerns of persistent coloring pollutants of textile industry wastewater and treatment approaches for environmental safety, J. Environ. Chem. Eng. 9 (2) (2021), 105012.
[5] M. Li, et al., Concentration and recovery of dyes from textile wastewater using a self-standing, support-free forward osmosis membrane, Environ. Sci. Tech. 53 (6) (2019) 3078–3086.
[6] E. Asgari, et al., Application of a photocatalytic ozonation process using TiO2 magnetic nanoparticles for the removal of Ceftazide from aqueous solutions: evaluation of performance, comparative study and mechanism, Optik 212 (2020), 164667.
[7] M. Jiang, et al., Conventional ultrafiltration as effective strategy for dye/salt fractionation in textile wastewater treatment, Environ. Sci. Tech. 52 (18) (2018) 10698–10708.
[8] G. Han, et al., Low-pressure nanofiltration hollow fiber membranes for effective fractionation of dyes and inorganic salts in textile wastewater, Environ. Sci. Tech. 52 (6) (2018) 3676–3684.
[9] M.R. Esfahani, et al., Nanocomposite membranes for water separation and purification: fabrication, modification, and applications, Sep. Purif. Technol. 213 (2019) 465–499.
[10] A. Aghaei, et al., The implications of 3D-printed membranes for water and wastewater treatment and resource recovery, Can. J. Chem. Eng. 100 (9) (2022) 2309–2321.
[11] S. Mohammad Nejad, et al., Loose nanofiltration membranes functionalized with in situ-synthesized metal organic framework for water treatment, Mater. Today Chem. 24 (2022), 100909.
[12] Y. Li, et al., Loose nanofiltration membrane with highly-branched SPEI/PEI assembly for dye/salt textile wastewater treatment, J. Environ. Chem. Eng. 9 (6) (2021), 106371.
[13] M.D. Firouzjaei, et al., Recent advances in functionalized polymer membranes for biofouling control and mitigation in forward osmosis, J. Membr. Sci. 596 (2020), 117604.
[14] M. Dadashi Firouzjaei, et al., Functionalized polyamide membranes yield suppression of biofilm and planktonic bacteria while retaining flux and selectivity, Sep. Purif. Technol. 282 (2022), 119981.
[15] M. Dadashi Firouzjaei, et al., MXenes: the two-dimensional influencers, Materials Today Advances 13 (2022), 100202.
[16] A. Zirehpour, et al., The impact of MOF feasibility to improve the desalination performance and antifouling properties of FO membranes, RSC Adv. 6 (74) (2016) 70174–70185.
[17] M.D. Firouzjaei, et al., Exploiting synergetic effects of graphene oxide and a silver-based metal-organic framework to enhance antifouling and anti-biofouling properties of thin-film nanocomposite membranes, ACS Appl. Mater. Interfaces 10 (49) (2018) 42967–42978.
[18] S.F. Seyedpour, et al., Toward sustainable tackling of biofouling implications and improved performance of tfc fo membranes modified by ag-mof nanorods, ACS Appl. Mater. Interfaces 12 (34) (2020) 38285–38298.
[19] H. Alamgholiloo, et al., A facile strategy for designing core-shell nanocomposite of ZIF-67/Fe3O4: a novel insight into ciprofloxacin removal from wastewater, Process Saf. Environ. Prot. 147 (2021) 392–404.
[20] M. Pejman, et al., Improved antifouling and antibacterial properties of forward osmosis membranes through surface modification with zwitterions and silver-based metal organic frameworks, J. Membr. Sci. 611 (2020), 118352.
[21] A. Rahimpour, et al., Simultaneous improvement of antimicrobial, antifouling, and transport properties of forward osmosis membranes with immobilized highly-compatible polyrhodanine nanoparticles, Environ. Sci. Tech. 52 (9) (2018) 5246–5258.
[22] W.-H. Zhang, et al., Graphene oxide membranes with stable porous structure for ultrafast water transport, Nat. Nanotechnol. 16 (3) (2021) 337–343.
[23] M. Zhang, et al., Controllable ion transport by surface-charged graphene oxide membrane, Nat. Commun. 10 (1) (2019) 1–8.
[24] Z. Lu, et al., Heterostructure design of carbon fiber@graphene@layered double hydroxides synergistic microstructure for lightweight and flexible microwave absorption, Carbon 197 (2022) 466–475.
[25] Y. Wang, et al., Controllable heterogeneous interfaces of cobalt/carbon nanosheets/ rGO composite derived from metal-organic frameworks for high-efficiency microwave attenuation, Carbon 187 (2022) 404–414.
[26] Y. Wang, et al., Metal organic frameworks-derived Fe-Co nanoporous carbon/graphene composite as a high-performance electromagnetic wave absorber, J. Alloy. Compd. 785 (2019) 765–773.
[27] M. Dadashi Firouzjaei, et al., Experimental and molecular dynamics study on dye removal from water by a graphene oxide-copper-metal organic framework nanocomposite, J. Water Process Eng. 34 (2020), 101180.
[28] M.D. Firouzjaei, et al., A novel nanocomposite with superior antibacterial activity: a silver-based metal organic framework embellished with graphene oxide, Adv. Mater. Interfaces 5 (11) (2018) 1701365.
[29] Y. Rezaeipour, et al., The anticancer properties of metal-organic frameworks and their heterogeneous nanocomposites, Biomaterials Advances 139 (2022), 213013.
[30] S.F. Seyedpour, et al., Tailoring the biocidal activity of novel silver-based metal azolate frameworks, ACS Sustain. Chem. Eng. 8 (20) (2020) 7588–7599.
[31] B. Hashemzadeh, et al., Degradation of ciprofloxacin using hematite/MOF nanocomposite as a heterogeneous fenton-like catalyst: a comparison of composite and core– shell structures, Chemosphere 281 (2021), 130970.
[32] J. Lee, et al., Graphene oxide nanoplatelets composite membrane with hydrophilic and antifouling properties for wastewater treatment, J. Membr. Sci. 448 (2013) 223–230.
[33] G. Yang, et al., A Sm-MOF/GO nanocomposite membrane for efficient organic dye removal from wastewater, RSC Adv. 10 (14) (2020) 8540–8547.
[34] P. Zhang, et al., Ultrathin reduced graphene oxide/MOF nanofiltration membrane with improved purification performance at low pressure, Chemosphere 204 (2018) 378–389.
[35] H.G. Alemayehu, et al., Highly stable membrane comprising MOF nanosheets and graphene oxide for ultra-permeable nanofiltration, J. Membr. Sci. 652 (2022), 120479.
[36] N. Bazrafshan, et al., Preparation and modification of low-fouling ultrafiltration membranes for cheese whey treatment by membrane bioreactor, Case Stud. Chem. Environ. Eng. 4 (2021), 100137.
[37] Y. Ouyang, et al., Poly-l-lysine-modified reduced graphene oxide stabilizes the copper nanoparticles with higher water-solubility and long-term additively antibacterial activity, Colloids Surf. B Biointerfaces 107 (2013) 107–114.
[38] C.-H. Kang, et al., Synthesis of ZIF-7/chitosan mixed-matrix membranes with improved separation performance of water/ethanol mixtures, J. Membr. Sci. 438 (2013) 105–111.
[39] Y.S. Li, et al., Molecular sieve membrane: supported metal–organic framework with high hydrogen selectivity, Angew. Chem. 122 (3) (2010) 558–561.
[40] Y. Wang, et al., Amino-functionalized ZIF-7 embedded polymers of intrinsic microporosity membrane with enhanced selectivity for biogas upgrading, J. Membr. Sci. 602 (2020), 117970.
[41] M. He, et al., Synthesis of zeolitic imidazolate framework-7 in a water/ethanol mixture and its ethanol-induced reversible phase transition, ChemPlusChem 78 (10) (2013) 1222–1225.
[42] Y. Lu, et al., Development of coin-shaped ZIF-7 functionalized superhydrophobic polysulfone composite foams for continuous removal of oily contaminants from water, J. Hazard. Mater. 421 (2022), 126788.

[43] D. Dahnum, et al., Formation of defect site on ZIF-7 and its effect on the methoxycarbonylation of aniline with dimethyl carbonate, J. Catal. 380 (2019) 297–306.
[44] W. Fu, et al., Visualizing and quantifying the nanoscale hydrophobicity and chemical distribution of surface modified polyethersulfone (PES) membranes, Nanoscale 9 (40) (2017) 15550–15557.
[45] E. Costa, et al., Chitosan nanoparticles as alternative anti-staphylococci agents: bactericidal, antibiofilm and antiadhesive effects, Mater. Sci. Eng. C 79 (2017) 221–226.
[46] M. Mozafari, et al., Facile Cu-BTC surface modification of thin chitosan film coated polyethersulfone membranes with improved antifouling properties for sustainable removal of manganese, J. Membr. Sci. 588 (2019), 117200.
[47] S. Chao, et al., Preparation of polydopamine-modified zeolitic imidazolate framework-8 functionalized electrospun fibers for efficient removal of tetracycline, J. Colloid Interface Sci. 552 (2019) 506–516.
[48] M. Pejman, et al., In situ ag-mof growth on pre-grafted zwitterions imparts outstanding antifouling properties to forward osmosis membranes, ACS Appl. Mater. Interfaces 12 (32) (2020) 36287–36300.
[49] M.F. Ismail, B. Khorshidi, M. Sadrzadeh, New insights into the impact of nanoscale surface heterogeneity on the wettability of polymeric membranes, J. Membr. Sci. 590 (2019), 117270.
[50] M.F. Ismail, et al., Surface characterization of thin-film composite membranes using contact angle technique: Review of quantification strategies and applications, Adv. Colloid Interface Sci. (2021), 102524.
[51] M. Pejman, et al., Effective strategy for UV-mediated grafting of biocidal Ag-MOFs on polymeric membranes aimed at enhanced water ultrafiltration, Chem. Eng. J. 426 (2021), 130704.
[52] P. Karami, et al., Nanodiamond-decorated thin film composite membranes with antifouling and antibacterial properties, Desalination 522 (2022), 115436.
[53] Y. Zhang, et al., A novel zinc complex with antibacterial and antioxidant activity, BMC chemistry 15 (1) (2021) 1–12.
[54] M. Ramani, S. Ponnusamy, C. Muthamizhchelvan, From zinc oxide nanoparticles to microflowers: a study of growth kinetics and biocidal activity, Mater. Sci. Eng. C 32 (8) (2012) 2381–2389.